SPE 102915

Magnetic Resonance Imaging of Methane - Carbon Dioxide Hydrate Reactions in Sandstone Pores

Graue, A., Kvamme, B. /U. of Bergen, Baldwin, B.A. /Green Country Petrophysics LLC, Stevens, J., Howard, J. /ConocoPhillips, Ersland, G., Husebø, J. /U. of Bergen, Zornes, D.R. /ConocoPhillips

This paper was prepared for presentation at the 2006 SPE Annual Technical Conference and Exhibition held in San Antonio, Texas, U.S.A., 24–27 September 2006.

Abstract

Formation and growth of methane hydrates in porous sandstone was monitored using Magnetic Resonance Imaging (MRI). A series of 3-D MRI images collected during these experiments illustrated patterns of hydrate growth. Calibrated MRI intensity changes that occured during the hydrate growth correlated with methane gas consumption and gave dynamic and quantitative in-situ information on hydrate formation rate and spatial distribution of the hydrate formed. Gas permeability was measured at various hydrate saturations and during hydrate growth. Experimentally it was verified that methane hydrate in porous sandstone spontaneously converted to CO_2 hydrate when exposed to liquid CO_2 at high pressure and low temperature. It has experimentally been determined that without heating, an exchange process between CO_2 and methane occured allowing the injected CO_2 to be stored as hydrate resulting in spontaneous production of methane, with no associated water production. The MRI images provided quantitative information on the methane production rates and amounts of methane released during the CH_4-CO_2 hydrate exchange reaction. Thermodynamic simulations based on Phase Field theory supported the measured results and predicted similar methane production rates observed in several reproduced experiments.

Introduction

Light hydrocarbon gases and water at high pressures and low temperatures may form hydrate structures, i.e. clathrates where water molecules encapsulate hydrocarbon molecules in rigid lattices. This solid occurs naturally at deep ocean floors, below sub marine bottoms and in permafrost regions. Hydrates have recently produced a lot of interest for different reasons; the net flux of methane released from underground hydrate accumulations reaching the atmosphere represents an environmental concern since methane is a more aggressive greenhouse gas (~ 25 times) than CO_2, and serious concern is related to the stability of these hydrate formations. Changes in local conditions of temperature, pressure or surrounding fluids or minerals change the dynamics of the system and might eventually lead to massive dissociation. The environmental impacts related to large amounts of methane released to the atmosphere may have dramatic effects on the greenhouse scenario. Another aspect of hydrate concern is the formation and dissociation of hydrates in relation to petroleum production activities; representing challenges for safe drilling operations and petroleum production and efficient gas transport. Increased use of sub-sea installations and ocean floor constructions raises concern to safety issues as discussed by Yakushev & Collett [1, 2].

Finally, due to the condensed presence of natural gas in hydrate layers, 1 cu. ft. of hydrate corresponds to approximately 163 cu. ft at atmospheric conditions, hydrate accumulations are viewed as potentially large energy resources. The abundance and locations of the natural gas hydrate reserves covers all continents with the total energy corresponding to natural gas entrapped in hydrate reservoirs estimated to be more than twice the energy of all known energy sources of coal, oil and gas [3]. Conventional production of natural gas from hydrate accumulations by pressure depletion in an underlying gas zone generates a large amount of associated water production, representing a significant environmental problem and limits the economic potential.

Thermodynamically CO_2 hydrate formation is more favorable compared to methane hydrate formation and this fact has initiated a study to determine if methane may be released from methane hydrates by exposing methane hydrate to liquid CO_2 [4].

In the present laboratory study Magnetic Resonance Imaging (MRI) has been used to follow the dynamics of hydrate formation and exchange in porous sandstone. The paper emphasizes first the experimental procedures developed to form methane hydrate in porous sandstone while monitoring the dynamic process with 3D imaging at a millimetre scale and then determine the production of methane from methane hydrate, when exposed to liquid CO_2, without external heating.

Hydrate Formation, Dissociation and Reformation

In controlled laboratory experiments gas hydrate was formed in porous rock. Two outcrop Bentheim sandstone core plugs, 9.4 cm long and 3.8 cm diameter, were used as reservoir rock in this study. Porosity and fluid permeability of the core plugs were measured at 22% and 1.1 Darcy, respectively for both plugs. The mineralogy for this sandstone shows 99% quartz content.

The first core plug was initially placed in a core holder in the MRI and vacuum evacuated. The core holder was made of composite material to minimize influence on the imaging capabilities. A cooling system was constructed that could hold the core at a selected, stable temperature within the range of 0-200ºC, with an accuracy of 0.1ºC, for an extended period of time. Figure 1 shows schematically the experimental set-up. The cooling fluid selected, Fluorinert (FC-84), is invisible to MRI and is also used as the confining fluid for pressure maintenance in the core holder. To keep the volume of the confining fluid small and the cooling bath and pumps at a safe distance from the magnet a heat exchange system was used. The tubing which circulated the high-pressure confining fluid was embedded in larger PVC tubing filled with the temperature controlled circulating propolene glycol, which was not piped through the MRI. The core plug was then pressurized to 81.6 bar using methane and exposed to brine injection from one end. The water flooded core reached a uniform saturation of 50% water and 50% methane. High spatial resolution fluid saturation imaging, at millimetre scale, was used to ascertain uniform water saturation distribution and was then applied when lowering the temperature for the system from ambient conditions to 4ºC to allow hydrates to form; a cooling that lasted for approximately 5 hours.

After heating and cooling the system several times the formation and dissociation of hydrates were monitored as function of time. During hydrate formation decreasing signal intensity is observed due to water forming a solid phase in the form of hydrate. By observing the lack of signal from the water phase dynamic 3D images of hydrate formation are obtained. Figure 2 shows that the hydrate measurable with MRI in the first core plug took several hours to form. The hydrate formation initiated at the end connected to a continuous supply of methane. Hydrate formation occurred as a frontal advancement from the inlet end towards the outlet end. The experiments were carried out at two different temperatures, first at 3ºC, then again at 5ºC, to be certain that no ice was formed in the aqueous phase. Various patterns of growth were observed, both as a front progressing from one end and a gradual loss of MRI signal throughout the core plug; the latter indicating a uniform distribution of hydrate growth. Most experiments formed hydrate thoroughout the core plug. Excellent results were obtained when comparing MRI intensity and methane consumption during hydrate formation as illustrated in Figure 3. Key parameters in these experiments include S_{wi}, composition and distribution of water (0.2 – 1.0) and distribution and supply of CH_4.

As in earlier MRI experiments of bulk hydrate [5,6], MRI was found to provide excellent resolution between the hydrate and its liquid/gas precursors and allowed the dynamic, spatial imaging of the formation and dissociation of hydrates in the porous sandstone under various injection conditions.

Gas Permeability in Gas-Water-Hydrate Systems

A series of experiments measured gas permeability in sandstone plugs during and after hydrate formation in rocks with various initial water saturations, between 33 and 52 percent.

Gas permeability was measured at steady-state flow of methane or nitrogen through the hydrate-bearing core sample. Figure 4 shows the change in permeability during stages of hydrate growth at 47 percent initial water saturation. Hydrate growth is shown as the fractional amount of free water, normalized to the initial (free) water saturation. Gas permeability decreases rapidly as hydrate forms. The reduction in permeability is explained from pore-filling reduction of porosity as hydrates expand and act as an extension of the solid grain space. Theoretical considerations imply that water molecules with entrapped CH_4 take up 26 percent more of the pore space when converted to hydrate. Clearly, the resistance to flow, which depends on hydrate microgeometry and growth pattern [7] will increase as the hydrate saturation increases and eventually occupies a portion of the pore space large enough to render the core impermeable. Figure 5 shows gas permeability results from five hydrate growth experiments. At high hydrate saturation (~ 62% PV) the gas permeability is reduced to a few mD in a 1.1 Darcy core. The results shown in Figure 5, not corrected for Klinkenberg, Forchhheimer and temperature effects, demonstrate significant gas permeability even at hydrate saturations above 60%. It is believed that hydrate growth patterns will strongly affect the relative permeability curves for water-gas-hydrate systems. Factors controlling the latter may include mineralogy and texture, water salinity, gas composition, and whether hydrate forms from free or dissolved gas [7]. The obtained results are relevant to situations where water is exposed to free methane; situations where hydrate preferentially starts forming on the gas-water interface.

Methane Production by CO_2 Sequestration

A second core plug was cut along the long axis into two half cylinders in order to establish an open fracture. This maximizes the surface area of the rock's water/gas mixture, and later the in-situ hydrate, to be exposed to the subsequent injection of liquid CO_2. When assembled in the core holder, a polyethylene spacer with two open and connected compartments was inserted in between the two half cores (Figure 6). To establish methane hydrates within the fractured porous media, the rock was saturated with pressurized methane then water was allowed to imbibe into the matrix, supplied from the fracture, until the water saturation reached a predetermined value. Brine injection was terminated when the water front approached the outlet end of the core in order to establish an area downstream with decreasing water saturation. Then the system was cooled to 4ºC to promote the formation of hydrates. Figure 7 shows the dynamic development of methane and water forming hydrates within the fractured, second core plug.

At the first time step shown in Figure 7 the core exhibits the saturation distribution obtained after the spontaneous brine imbibition was terminated. A limited, predetermined amount of water had been injected into the fracture, and was allowed to imbibe into the two half cores

resulting in a 50% water saturation. Trapped methane in the invaded pore space and free methane in the upper part of the core halves were supported by available free methane from the fracture and the methane source when being consumed during the subsequent hydrate formation; when the temperature was lowered. Since the MRI signal represents the water, a lack of signal indicates that the water had solidified into hydrates. At 60 hours the hydrate formation ceased and it is seen that at the plug end containing the dispersed, or decreasing, water saturation only partly hydrate formation was observed. Down stream, in the region of free methane gas saturation with no water present, no hydrate is formed. Free methane is not detected within the porous rock by MRI; however, in bulk it is possible to measure the methane concentration, due to longer relaxation times. Therefore, a stable concentration of methane is observed in the fracture during the hydrate formation as a methane source was readily available at the up stream end of the core plug.

CO_2 was injected into the fracture to flush out the methane and allowed to interact with the hydrate. The subsequent kinetic interaction with the hydrate is shown in Figure 8. As can be seen from this figure methane was spontaneously produced into the fracture, as later was verified from effluent analysis. A profile of the MRI intensity generated from the methane concentration along the length of the fracture as a function of time gave in-situ information on the amount of methane produced. The noticeable difference in the change of the MRI intensity along the length of the fracture suggested that the methane production continued over 4 days. When no increase in methane concentration could be observed, a CO_2 flush of the fracture was performed. Figure 9 exhibits the in-situ methane production, measured by MRI, as function of time between each CO_2 flush. It is noticeable from Figure 9 that the methane production rate was very similar for all of the three productions; early fairly high then slowly decreasing. The production of methane ceased earlier for each subsequent CO_2 flush. The latter may indicate that the amount of methane hydrate contacted by CO_2 was reduced after each CO_2 flush while the former is, as indicated above, related to changes in chemical potential of CO_2 and the kinetic effects of reduced thermodynamic driving force on the methane production. When methane production ceased, a CO_2 flush of the fracture was performed and the effluent was characterized by gas chromatography. This sequence of flushing procedures was performed 2-4 times to allow for additional methane production. Figure 9 includes the effluent methane production by material balance calculations from three CO_2 flushes.

At the experimental P-T conditions the density of pure methane is typically gas phase density in contrast to pure CO_2 which is in the liquid region at the same conditions. The relative buoyancy of a separate CH_4 phase relative to a separate CO_2 phase is reduced due to mutual solubility of the two components, which for intermediate concentration ranges will lead to phase separation. Practically this means that the escape of released CH_4 may be limited by the kinetics of CH_4 dissolution into the CO_2 phase, and eventually a phase split, depending on the relative amounts of CH_4 and CO_2 at the local conditions of temperature and pressure. This implies that the production rate is determined both by the reduced available methane hydrate and also by reduced thermodynamic driving force caused by the dilution and phase splitting of the CO_2 phase in the spacer compartment. In a real reservoir with channels/fractures the escape of CH_4 will thus be a complex function of the local conversion kinetics and the local flow situation. Natural hydrate structures vary significantly. A typical pattern is that the hydrate layers are separated by low permeable clay layers. Hydrate layers can be considered as more or less a stationary structure which is typically not thermodynamically stable in a rigorous sense but rather trapped into a situation of slow dynamics. In addition to the presence of fractures in the sediment structure, as well as in the trapping layers above, the success of a natural CH_4 replacement scenario depends on the type of sediment and corresponding flow properties. Practically these issues as well as the extension and connectivity of the hydrate layers are key factors in determining the actual value of a hydrate reservoir as a storage site with corresponding natural gas production.

Conclusions

- The dynamics of methane hydrate formation in sandstone have been monitored with MRI.
- Spontaneous conversion of methane hydrate to CO_2 hydrate was implied by the production of methane when the hydrate was exposed to liquid CO_2.
- The conversion of methane hydrate into carbon dioxide hydrate in sandstone takes place without adding heat to the system.
- Within the scale of the MRI resolution no liquid water phase was observed.

Acknowledgement

Several of the authors are indebted for the support from the Royal Norwegian Research Council. The authors acknowledge the permission from ConocoPhillips to publish this work.

References

1. Yakushev, V.S., Collett, T.S. Gas hydrates in arctic regions: Risk to drilling and production. *Proc. 2nd Int. Offshore and Polar Engineering Conference*, San Francisco, USA (1992).

2. Dawson, A.G., Long. D., Smith. D.E. The Storegga slides: Evidence from eastern Scotland for a possible tsunami. *Marine Geology*, **82**, 271-276 (1988)

3. Sloan, E.D. Fundamental principles and applications of natural gas hydrates. *Nature*, **426** (2003).

4. Graue, A., Kvamme, B., Baldwin, B.A., Stevens, J., Howard, J., Aspenes, E., Ersland, G., Husebø, J., Zornes, D.R.: "Environmental Friendly CO_2 Storage in Hydrate Reservoirs Benefits from Associated Natural Gas Production", SPE 18087, *Proc.: 2006 Offshore Technology Conference*, Houston, TX, USA, May 1-4 (2006).

5. Moudrakovski, I.L., Ratcliffe, C.I. and Ripmeister, J.A. Application of magnetic resonance microimaging (mrm) to monitor the formation of gas hydrate. *Proc.: Fourth International Conference on Gas Hydrates*, Yokohama, Japan, May 19-23 (2002).

6. Baldwin, B.A., Moradi-Araghi, A. and Stevens, J.C. Monitoring hydrate formation and dissociation in sandstone

and bulk with magnetic resonance imaging. *Magnetic Resonance Imaging*, **21**, 1061-69 (2003).

7. R.L, Kleinberg, C.Flaum, D.D. Griffin, P.G. Brewer, G.E Malby, E.T. Peltzer, J.P. Yesinowski, Deap Sea NMR: Methane Hydrate Growth Habit in Porous Media and its Relationship to Hydraulic Permeability, Deposit Accumulation, and Submarine Slope Stability" submitted to Journal of Geophysical Research B, March 2003.

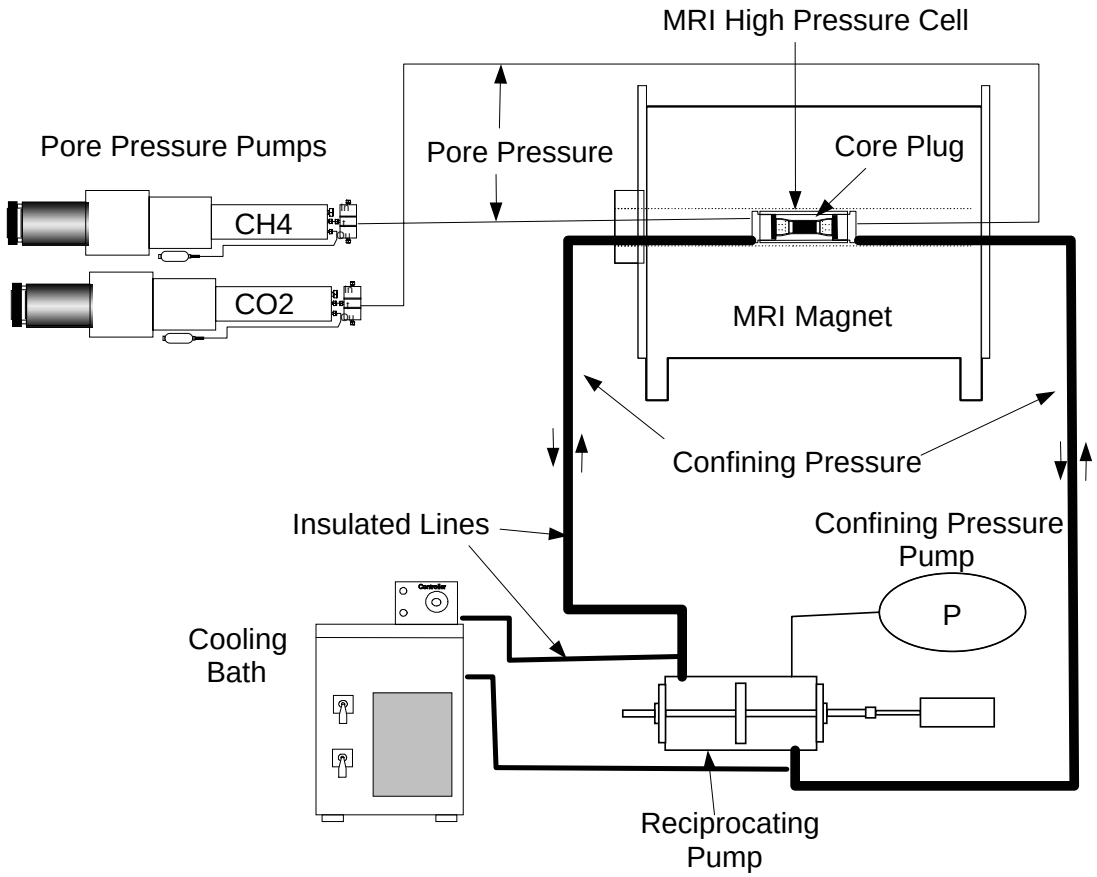

Figure 1. Schematics of the experimental set-up.

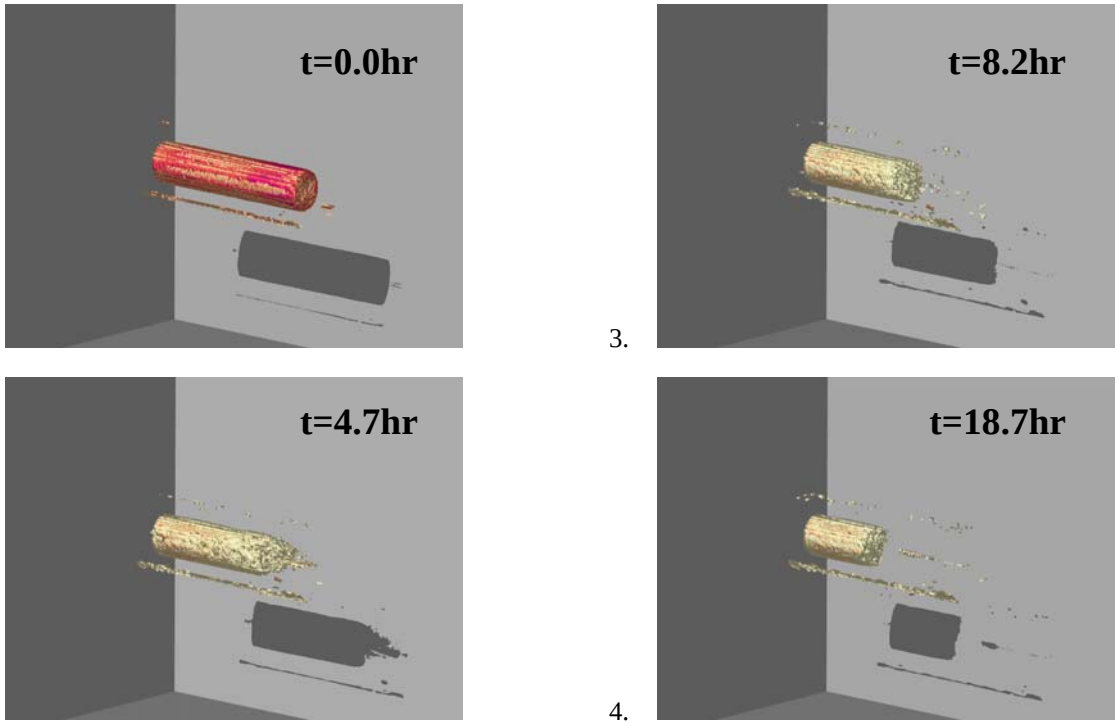

Figure 2 . Dynamics of hydrate formation in sandstone.

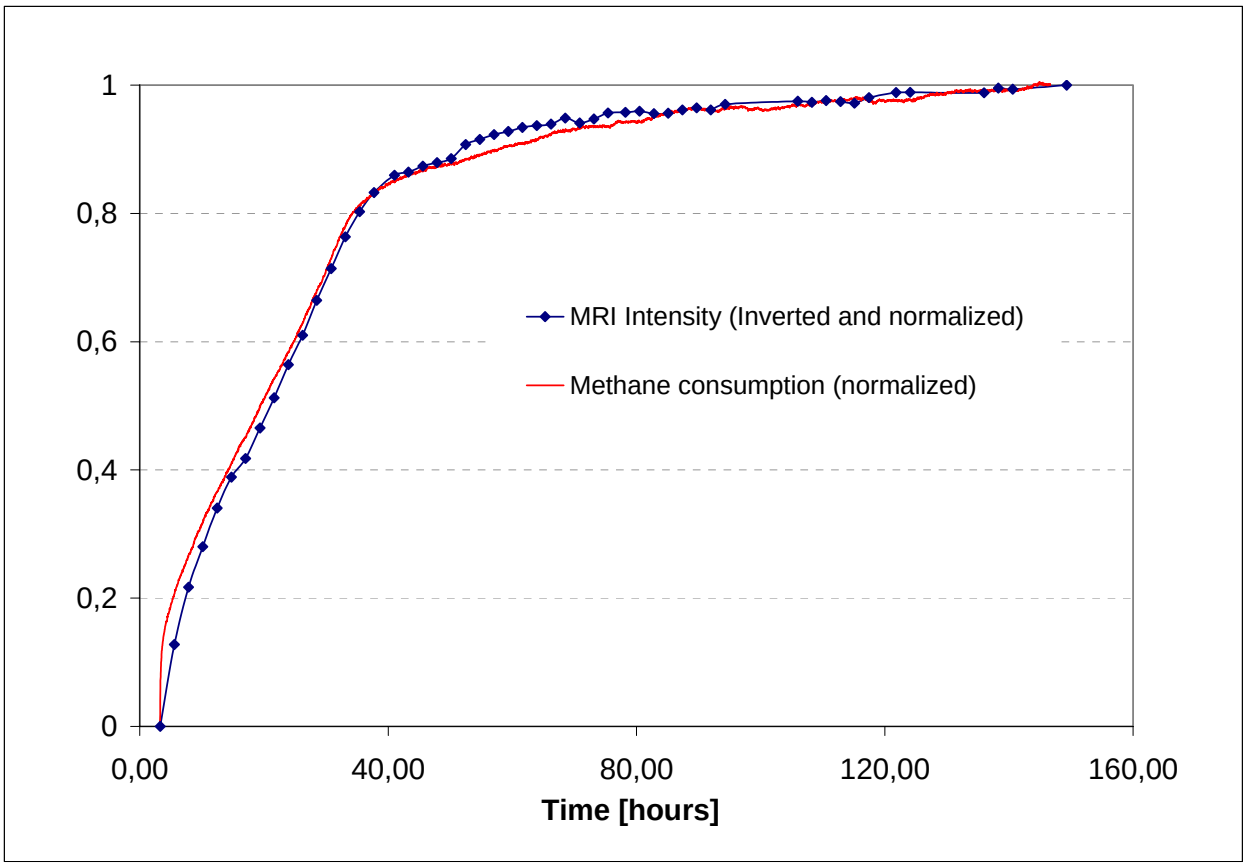

Figure 3. Comparison of MRI intensity and methane consumption during hydrate formation

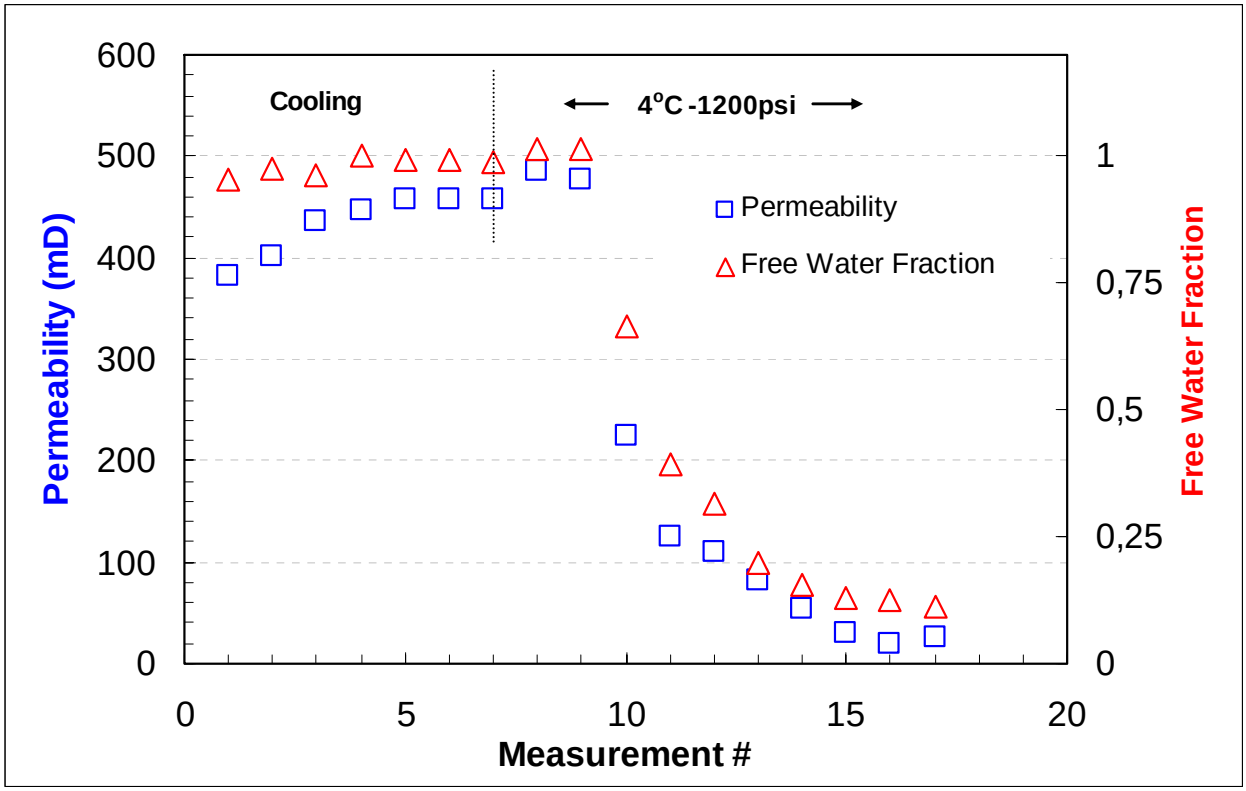

Figure 4. Gas permeability measured during hydrate growth, Swi=47 % PV.

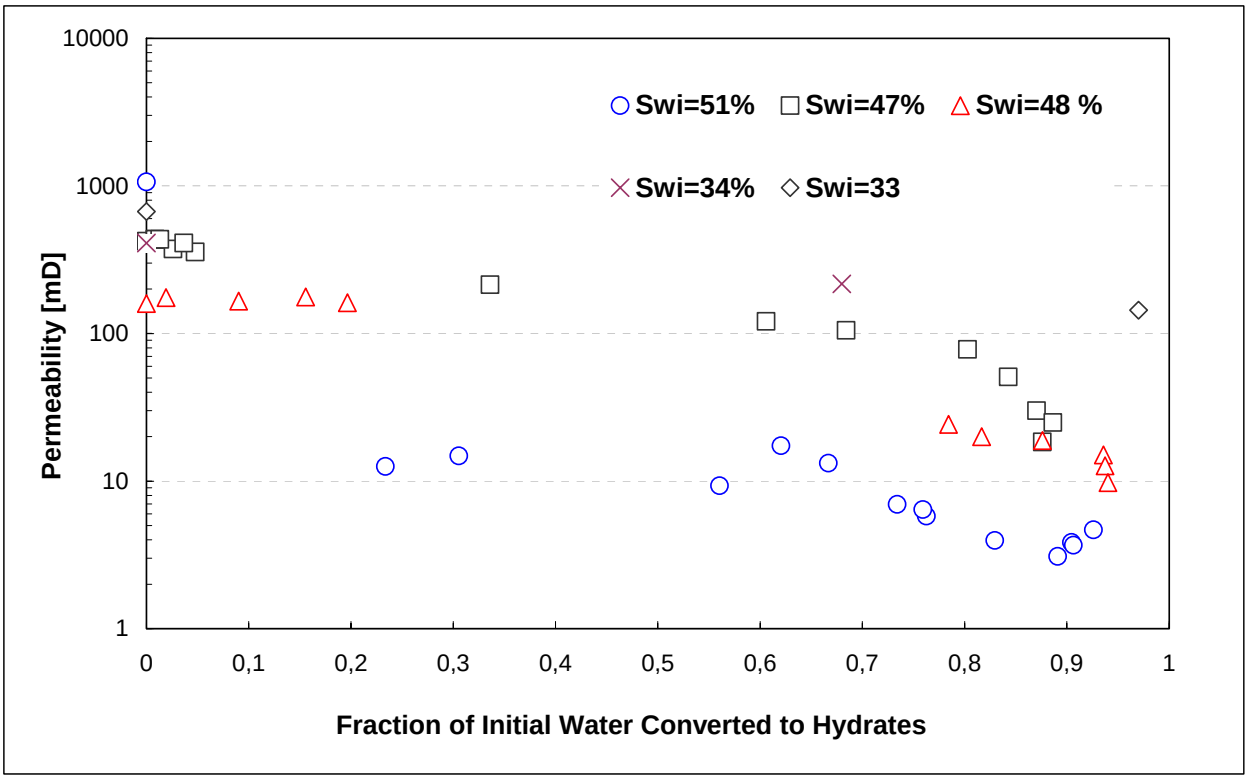

Figure 5. Gas permeability as function of amount of initial water converted to hydrate.

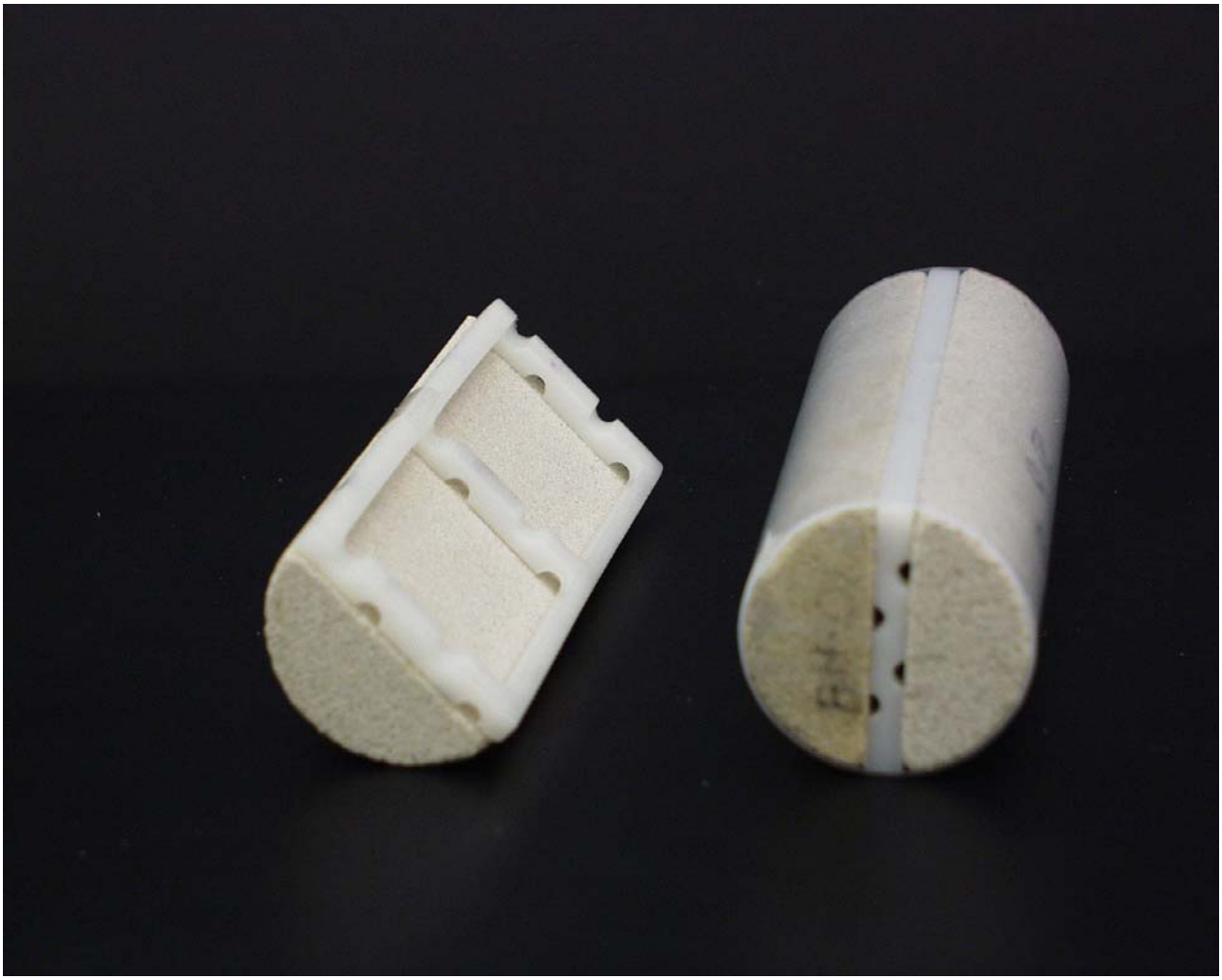

Figure 6. Spacer used to establish the fractured core plug assembly.

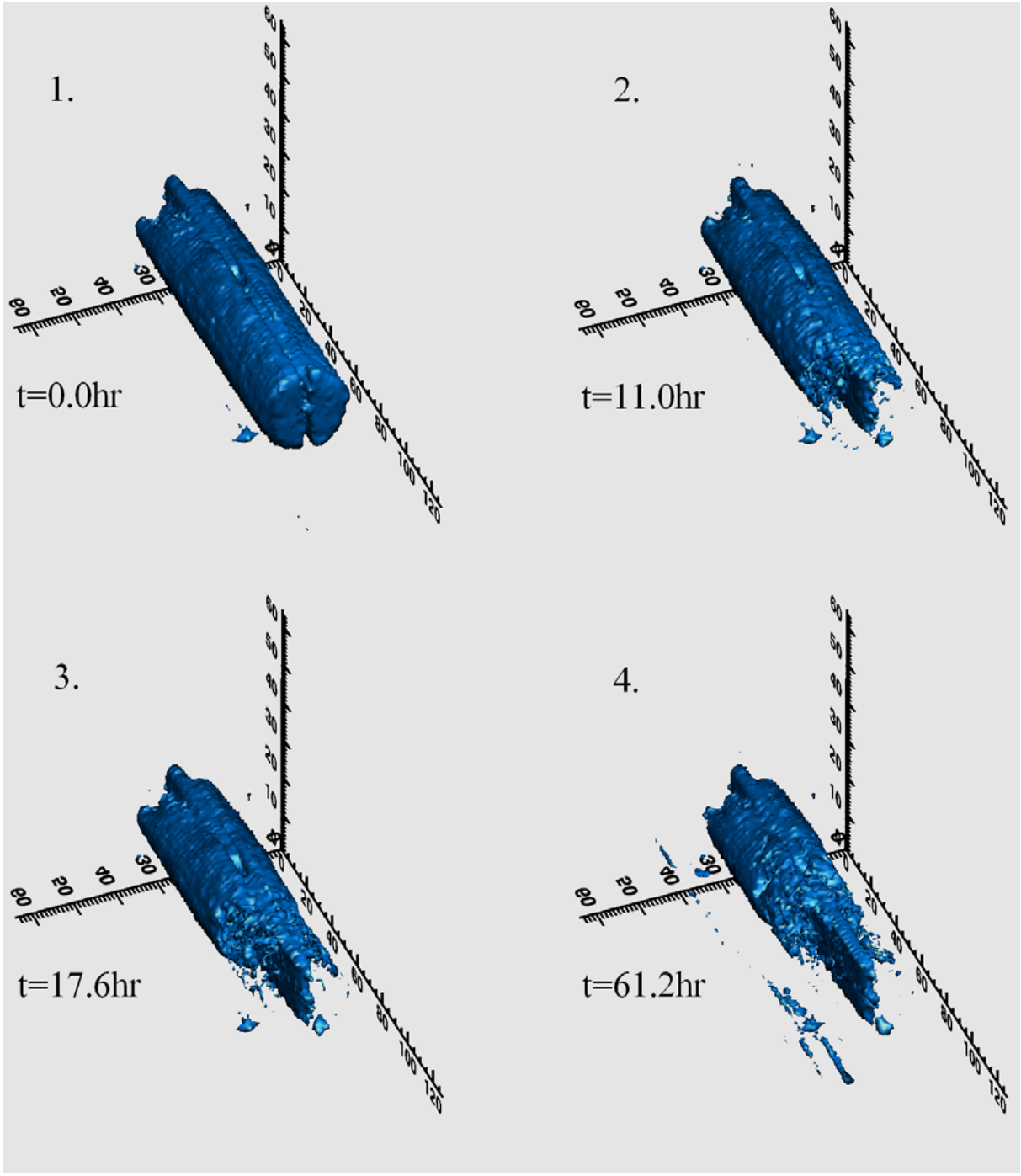

Figure 7. Hydrate formation in the fractured core plug at 4 time steps: 1) Started cooling sample to 4ºC. 2) Methane hydrate starts forming. 3) Continued hydrate formation; the free methane in the fracture is easily identified. 4) Hydrate formation rate decreasing.

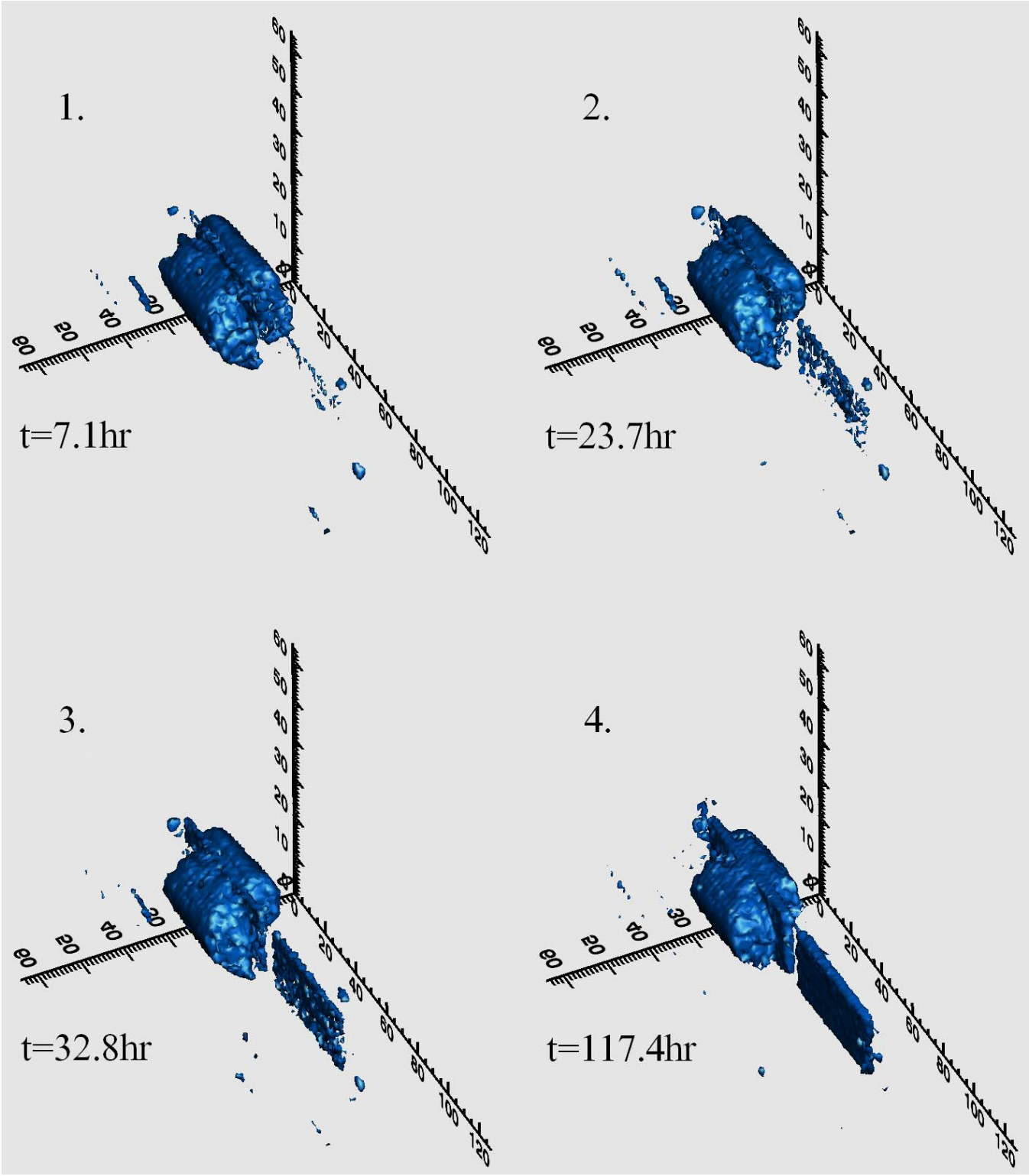

Figure 8. Methane production from the hydrate into the CO_2 filled fracture at 4 time steps: 1) The free methane in the fracture has been displaced by the liquid CO_2 flush. Time step 2, 3, and 4) CO_2 replaces methane in the hydrate and methane is produced into the fracture.

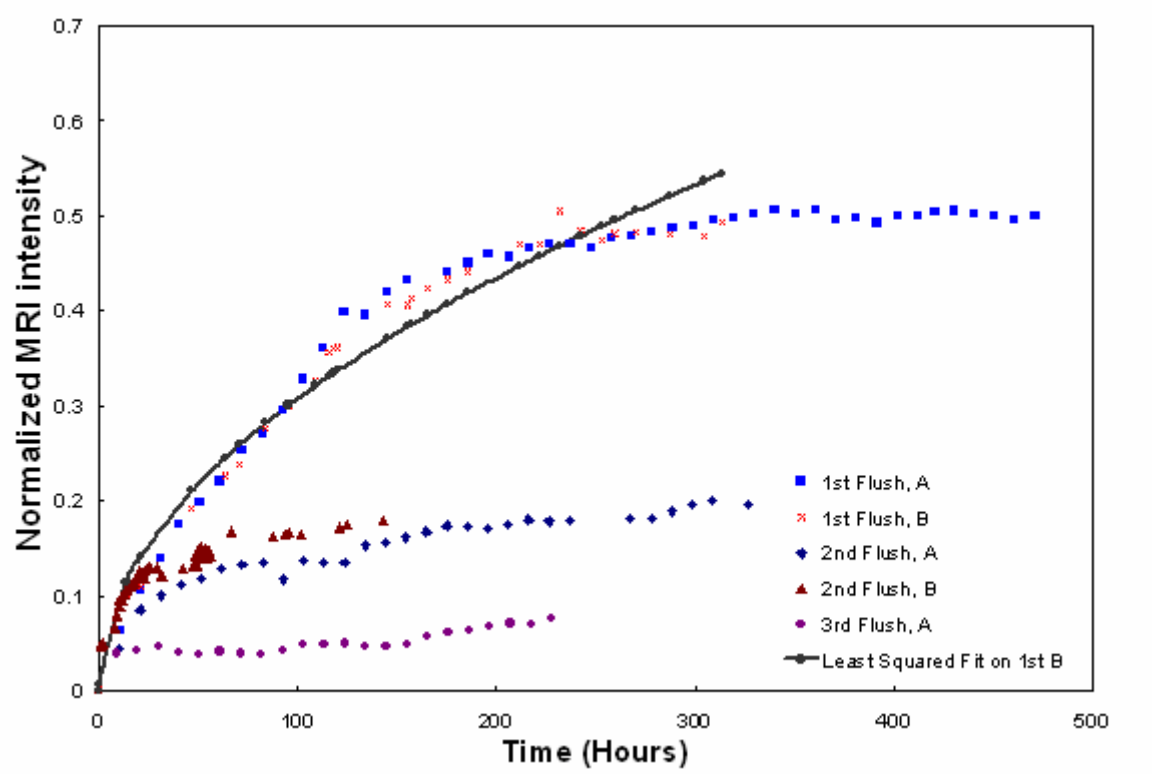

Figure 9. Methane production as function of time. A and B are two independent experiments and illustrate the reproducibility. The first flush is compared to an isothermal phase field simulation.